UKRAINIAN ASTRONOMICAL ASSOCIATION

MAIN ASTRONOMICAL OBSERVATORY
OF THE NATIONAL ACADEMY OF SCIENCES OF UKRAINE

with support

CRDF

INTAS

MINISTRY OF UKRAINE FOR EDUCATION AND SCIENCE

Astronomy in Ukraine – 2000 and Beyond

(Impact of International Co-operation)

Kyiv 2000

General Reports

CRDF ACTIVITIES WITH UKRAINE

N. Artiukhovskaya

CRDF-Kyiv
4 Bogomoltsa St., Suite 133
01024 Kyiv, Ukraine

The U.S. Civilian Research and Development Foundation for the Independent States of the former Soviet Union (CRDF) is a unique public-private partnership to support cooperative, R&D-related projects between U.S. scientists and engineers and their counterparts in the former Soviet Union. The mission of the CRDF is to fund civilian projects conducted in the U.S and in the countries of the former Soviet Union (fSU). These projects should help sustain outstanding fSU scientific and engineering research capability, promote defense conversion and contribute to the development of market economies in the region.

Since its operational inception in September 1995, the CRDF has established a strong working relationship with the Department of Science, Technology and Ecology of the Cabinet of Ministers of Ukraine and with the State Committee of Ukraine for Science and Intellectual Property (and its administrative predecessors). Ukraine's extraordinary commitment of up to $1.44 million to cooperative activities with the CRDF far exceeded the minimum requirement established by NSF ($156,045). It served as an example for other fSU counterparts to meet at least their minimum commitment to participate in CRDF programs. This relationship has been solidly defined by a series of MOU's and Decision Documents signed in December 1995, July 1996, October 1996, April 1997, and 1999.

CRDF has supported Ukrainian scientists with the following eight programs:

I. Cooperative Grants Program (CGP):

- Supports joint projects between scientists and engineers from the U.S. and countries of the former Soviet Union in all areas of civilian research and development. Grants provide individual financial support, equipment, and travel, with most overhead costs paid by Ukraine.
- Based on the results of CRDF's merit review, in April 1997, the CRDF and the Government of Ukraine announced 60 two-year awards at an average funding level of $45,107. Work conducted under these awards was completed by the end of 1999.
- This represents 21% of the 282 awards that CRDF has issued to all countries of the former Soviet Union under the original round of this Program.
- The original budgets for Ukrainian awards totaled $2,706,413, of which $1,361,678 was to be provided by CRDF and $1,344,735 was to be provided by Ukrainian sources. The actual amounts paid by CRDF and Ukraine respectively were $1,333,341 and $676,700.
- CRDF announced a second competition in June 1999. By the October 1, 1999 deadline, CRDF had received 225 proposals from Ukraine. This represents 18% of the total for the former Soviet Union of 1,250 proposals. CRDF plans to announce decisions on May 15, 2000. CRDF and the State Committee of Ukraine for Science and Intellectual Property have tentatively agreed to allocate up to $1.2 million, of which up to $1 million will be allocated by the CRDF, and the equivalent of $200,000 will be allocated by the Ukrainian side for supporting the Ukrainian host institutions.
- The US National Science Foundation (NSF) awarded CRDF an additional $160,000 to this program for two purposes: 1) provide stipends for Ukrainian young investigators participating on resulting CGP awards ($80,000); and 2) provide support for 4–5 scientific workshops in Ukraine which allow US and Ukrainian scientists

Number of the Projects Supported by the CRDF Programs in Ukraine

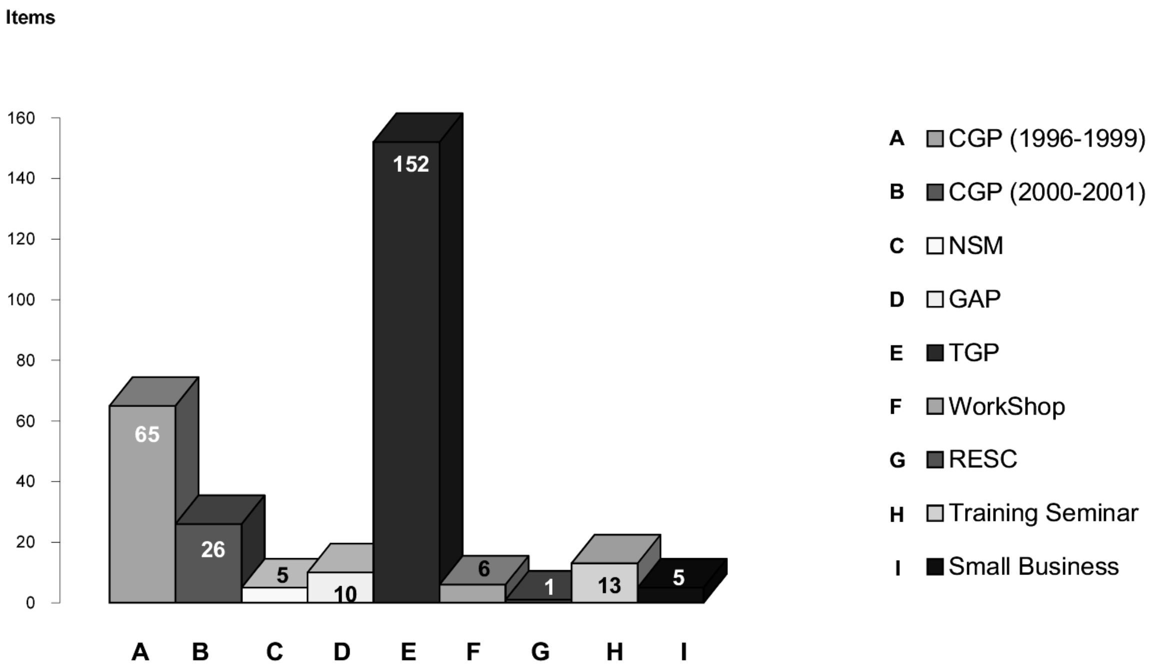

Funding of the CRDF Programs in Ukraine

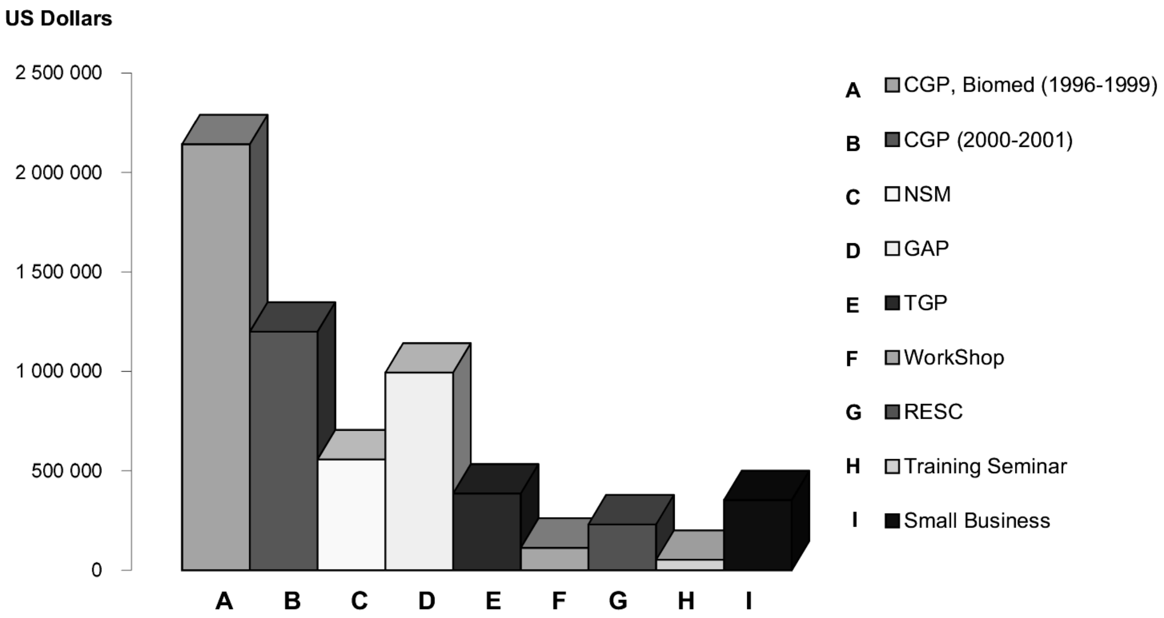

to meet and discuss potential new projects to be submitted to the NSF, CRDF, or other agencies. By the January 15, 2000 deadline, CRDF received 43 workshop proposals.

II. Travel Grants Program:

- This program offers up to $3,600 to promising young applied scientists and engineers from the former Soviet Union to facilitate their participation in selected meetings of industry associations and scientific and engineering professional societies in the United States.
- In the original round of this program, CRDF issued 141 travel grant awards to Ukrainian scientists totaling $346,201 (average grant: $2,455)
- This represented nearly 75% of the 193 total awards issued under the program.
- On June 1, 1999, CRDF initiated a modified version of the TGP, which provides travel support to fSU scientists strictly for the purposes of developing collaborations with U.S. businesses.
- CRDF announced a second round of the program on June 1, 1999.
- Under this round, CRDF has issued 11 awards to date to Ukrainian scientists for which it has obligated $39,600.

III. "Next Steps to the Market" Program:

- Program intended to stimulate cooperation in applied R&D through the support of projects designed to facilitate and expedite the commercial utilization of research results.
- Financial support under this program includes targeted additional investments to supplement existing CRDF awards, training, travel, and other appropriate measures.
- Projects are designed to include appropriate cost sharing by the U.S. partner.
- CRDF has awarded three Next Steps grants for cooperative R&D projects between Ukrainian researchers and American companies that were developed from contacts the Ukrainian scientists made while they were in the United States under auspices of the CRDF Travel Grants Program.
- CRDF has contributed $132,220 to these awards, with corporate partners contributing an additional $425,300 (though not all of this amount went to Ukrainian scientists).
- CRDF announced a second round of the program on June 1, 1999.

IV. Small Business R&D Cooperation Program (Now closed to new proposals)

- Through this program CRDF hopes to assist the creation and growth of high technology business and to stimulate economic growth in Ukraine. In addition, the program will provide a mechanism for Ukrainian scientists, engineers and entrepreneurs to better understand commercial business practices and will provide access for U.S. companies to significant Ukrainian scientific talent and technology.
- This pilot program consists of two types of awards: Travel Grants and R&D Collaborative Grants
- Travel Grants. This component of the program supported travel grants of $3,650 each for Ukrainian travelers. The grants enabled potential collaborators to meet and discuss the technology in question and its relevance to the business interests of both parties.
- In September 1998, CRDF made eleven (11) travel grant awards to Ukrainian scientists for travel to the United States to meet with representatives from U.S. Companies and discuss possible R&D collaborations.
- These travel grants resulted in fourteen (14) submissions to the Ukrainian Small Business Development Collaborative Grants Program.
- R&D Collaborative Grants for Small Business Partnerships. This component of the program provides technology development funding for partnerships involving Ukrainian and American small businesses (fewer than 500 employees).
- In April 1999, CRDF made five awards totaling $250,000 for U.S./Ukraine collaborations involving small, high technology businesses to support research and development activities designed to facilitate and expedite the commercial utilization of research results in the U.S. and Ukraine.
- U.S. companies contributed funding in the amount of $103,303 to projects in this program (though not all of this amount went to Ukrainian scientists).
- Experience in the operation of this program has enhanced planning for additional programs in this area.

V. Department of Commerce funded Training Program in Technology Development and Marketing:

- From March 1–5, 1999 with funding from the Department of Commerce and logistical support from the State Committee of Ukraine for Science and Intellectual Property, CRDF held a Technology Development and Marketing seminar in Kyiv for 14 competitively-selected Ukrainian scientists. A 15th Ukrainian participant attended a subsequent seminar in Yerevan.

- The seminar provided five days of training in the commercialization of technologies in the West for scientists in the Independent States. Practical and focused examples and advice were provided for three days on such topics as technology licensing, business plan development, patents and intellectual property. For two days, experts met with individual scientists to discuss their technology or process, and its commercial potential.
- CRDF is organizing one-week visits to the U.S. for 14 of the 15 Ukrainian participants to meet with potential U.S. business partners, participate in trade shows, and /or attend appropriate industry association meetings.

VI. Major Equipment for Regional Experimental Support Centers (RESC):

- Program aims to place major equipment at applied research centers where it can be used to carry out experiments underpinning technological development and sustainable economic growth on a regional basis.
- In Spring 1997, based on an expert review, CRDF announced award of a $231,000 Varian NMR Spectrometer to the Kavetsky Institute of Experimental Pathology, Oncology and Radiobiology in Kyiv.
- CRDF arranged for selected staff at the Institute to receive both facility management and technical training on the apparatus.
- This is one of seven RESC awards CRDF made throughout the former Soviet Union.

VII. Collaborations in Biomedical and Behavioral Sciences (Now closed):

- Supported collaborative research and development projects in the biomedical and behavioral sciences.
- Total funding was $1.5 million for all countries of the former Soviet Union.
- CRDF awarded five of the 43 two-year awards to Ukraine.
- The original budgets for these awards totaled $200,000, of which $100,000 was to be provided by the CRDF and $100,000 was to be provided by Ukraine. The actual amounts paid by CRDF and Ukraine respectively were $96,609 and $35,275.
- All awards were completed by the end of 1999, and CRDF is conducting an evaluation of the program.

VIII. Grant Assistance Program (GAP) 1998-Present

- GAP facilitates assistance efforts by public and private sector organizations in support of civilian scientific research, educational and charitable projects and activities in the former Soviet Union (fSU).
- GAP provides financial and administrative services to transfer and monitor project funds into the states of the former Soviet Union. Under this program the CRDF:
- Delivers project funds from Sponsor organizations directly to project participants into the fSU free of taxes.
- Provides support for the procurement and delivery of project equipment and supplies free of taxes and customs duties.
- Facilitates the arrangement of international travel.
- Provides detailed accounting to Sponsor organizations for all project funds administered by the CRDF.
- Only a few projects have been carried out in Ukraine, though CRDF believes the annual level of projects could easily approach $2–4 million given a clear and public tax exemption for such transfers and a clear, predictable and timely process to certify projects for tax-free treatment in Ukraine.

UV-ASTRONOMY: STATE-OF-ART AND PROSPECTIVE. CONTRIBUTION OF THE CRIMEAN ASTROPHYSICAL OBSERVATORY

R. E. Gershberg

Crimean Astrophysical Observatory, Ministry of Ukraine for Education and Science
Naukove, 98409 Crimea, Ukraine
e-mail: gershberg@crao.crimea.ua

The report consisted of a short review of the ASTRON mission that was described in details in the "Astrophysical studies with the space station ASTRON" (Moscow: Nauka, 1994) and of the SPECTRUM-UV project that was described in details by Gershberg R. E., Zvereva A. M., Petrov P. P., Pronik V. I., and Steshenko N. V. "The "Spectrum-UV" space project" in Space Science and Technology.–1995.–**1**, N 1.–P. 47.

Invited paper by Prof. Roald Gershberg, the UAA Laureate of 1997–2000 yrs "For the Outstanding Contribution for Advancement of Astronomy in Ukraine".

FIRST MAGNETOSPHERIC ECHO TRACES FROM THE RADIO PLASMA IMAGER ON IMAGE

B. W. Reinisch[1], D. M. Haines[1], I. A. Galkin[1], X. Huang[1], G. Sales[1], J. L. Green[2], R. F. Benson[2], S. F. Fung[2], W. W. L. Taylor[3], J.-L. Bougeret[4], R. Manning[4], P. H. Reiff[5], D. L. Carpenter[6], and D. L. Gallagher[7]

[1] *Center for Atmospheric Research, University of Massachusetts, Lowell, MA, USA*
e-mail: `Bodo_Reinisch@uml.edu`

[2] *NASA Goddard Space Flight Center, Greenbelt, MD, USA*

[3] *Raytheon ITSS Corporation, Lanham, MD, USA*

[4] *Observatoire de Paris, Meudon, France*

[5] *Rice University, Houston, TX, USA*

[6] *STAR Laboratory, Stanford University, Palo Alto, CA, USA*

[7] *NASA Marshall Space Flight Center, Huntsville, AL, USA*

The radio plasma imager (RPI) on the IMAGE satellite is a low-frequency radar system that uses orthogonal 500-m tip-to-tip dipoles to transmit RF pulses with frequencies from 3 kHz to 3 MHz. A third 20-m tip-to-tip dipole antenna along the spin axis is used for reception together with the two long antennas providing direction of arrival capability. The minimum pulse length of 3.2 ms yields a range resolution of 480 km. When the spacecraft is in the magnetospheric cavity (altitude of 5–7 RE) RPI can receive echoes associated with the plasmasphere, the magnetopause and the cusp region, at frequencies between $\sim$10 and 100 kHz. At high altitudes, higher frequency echoes are found reflecting from the topside ionosphere. This paper will present some of the first echo observations measured by the RPI instrument.

INTRODUCTION

The Imager for Magnetopause-to-Aurora Exploration (IMAGE) satellite was launched on March 25, 2000 into a highly elliptical polar orbit with an initial apogee geocentric radial distance of 8.22 RE and initial perigee of 1000 km. IMAGE is the first spacecraft dedicated to remote sensing of the magnetosphere (Burch, 2000). Observations from the IMAGE instruments are used to determine the global-scale structures and dynamics of the magnetosphere by imaging the aurora at several wavelengths, imaging the plasmasphere from resonance scattering He+, imaging neutral atoms from 10 eV to 500 KeV in energy, created by charge exchange with the Earth's neutral H exosphere, and by radio sounding with the Radio Plasma Imager (RPI).

The RPI instrument covers the frequency range from 3 kHz to 3 MHz with a receiver bandwidth of 300 Hz. RPI uses three orthogonal thin wire antennas, two 500-m tip-to-tip dipoles in the spin plane (X and Y), and a 20-m tip-to-tip dipole along the spin axis (Z). All RPI antennas are used for reception, allowing the measurement of the angle of arrival of the signals (Reinisch *et al.*, 1999). The X axis dipole is used for transmission and is electronically tuned to enhance the transmission efficiency. The radiated RF power is limited to 10 W. A number of different waveforms can be selected to adapt to diverse environments, *e.g.*, a simple 3.2 ms pulse modulation with constant repetition rate or a complimentary phase-coded pulse consisting of 4, 8, or 16 of the 3.2 ms chips. Selective application of pulse compression and spectral integration processing enhances the signal-to-noise ratio by nominally 15 dB. The design of the RPI is described in much greater detail by Reinisch *et al.*, 2000a and is based on the design of the "Digisonde" (Reinisch, 1996) that has successfully been used for years to monitor ionospheric density from the ground.

PASSIVE OBSERVATIONS WITH RPI

Radio sounding measurements with RPI are typically interspersed with passive operations (Oya *et al.*, 1990). The result is that a complete spectrum of passive measurements is generated at least once every eight minutes

Invited paper.

Figure 1: Frequency-time spectrogram of RPI passive measurements May 11, 2000. The green trace is the expected *in-situ* gyrofrequency obtained from a model magnetic field. Local density measurements can be easily determined since plasma thermal emissions, during times when the fg $\ll$ fp, are clearly seen and provide a plasma frequency map of the polar cusp and plasmasphere as shown in this example

Figure 2: RPI echoes from the high latitude magnetosphere are shown in these plasmagram plots of apparent range versus frequency. The apparent range is determined by assuming the echoes are due to electromagnetic pulses traveling at the speed of a light in vacuum and measuring the time delay between transmission and signal reception

Figure 3: Left-hand panel shows the plasmagram of echoes from the polar cusp. The right-hand panel shows the dynamic spectrogram of plasma emissions during *in-situ* measurements as the IMAGE spacecraft passed through the polar cusp over a several hour period

Figure 4: Whistler mode echoes are observed at frequencies below about 80 kHz

and sometimes every two or four minutes. These passive wave observations are used to provide a familiar context for the RPI echo observations and to measure the characteristic cutoff frequencies in the local plasma. In the passive mode, RPI measures the electric field intensity simultaneously from each of the three axis dipole antennas with three separate receivers. Figure 1 shows a typical RPI dynamic spectrogram from 9 to 300 kHz for May 11, 2000, as measured with the X-axis dipole. Due to RPI's long antennas and very low noise receivers the spectrograms provide a very rich set of wave observations. The green trace overlaying the spectrogram in Figure 1 is the local electron gyrofrequency (fg) as determined from a typical model field. Since IMAGE's orbital period is 14.25 hours, fg can be seen to go through nearly two complete cycles in 24 hours.

On May 11, 2000 RPI observed a number of solar type III radio bursts and auroral kilometric radiation (AKR). When IMAGE enters the cusp region or the plasmasphere, the ambient emissions can no longer propagate to the spacecraft and the sudden intensity cutoffs identify the local plasma frequencies. IMAGE's orbit is such that its apogee is on the day side at about 7 hours magnetic local time (MLT) at about 45° magnetic latitude.

For May 11, 2000 shown in Figure 1, RPI measured a number of echoes and local plasma resonances throughout its orbit. Typical echo traces will be presented in the next section.

MAGNETOSPHERIC ECHOES

Echoes from RPI transmissions are observed when IMAGE is located in a low-density region between higher-density regions (which could be the ionosphere, the plasmasphere, the magnetospheric cusp and the magnetopause). The primary presentation of RPI sounding data is in the form of plasmagrams, which are the magnetospheric analogs of ionograms. Figure 2 shows a sequence of three plasmagrams on May 11, 2000, when the IMAGE spacecraft is outgoing at large radial distance over the northern polar cap in the low density region of the magnetosphere. The plasmagram is a plot of the echo amplitude as a function of frequency and echo delay τ. Instead of τ the vertical axis shows $c\tau/2$, the so-called virtual range to the reflector since it assumes that the radio pulse propagates with the speed c of light in vacuum. The true distances from the satellite to the reflecting plasma can be calculated using an inversion algorithm developed for magnetospheric sounding (see Reinisch *et al.*, 2000b).

The echo traces in Figure 2 extend to higher time delays with increasing frequencies, and have a shallow slope from 200 kHz to nearly 1000 kHz, indicating a steep density gradient in the reflecting region of the polar cap. These panels all show two traces indicating that RPI is observing the ordinary and extraordinary mode echoes. Traces such as these have been observed for times exceeding two hours, allowing an unprecedented capability of determining the high latitude density structure and dynamics.

POLAR CUSP ECHOES

One of the key IMAGE science questions is the mechanism of injection of plasma into the magnetosphere. By comparing the cusp echoes shown in the left hand panel of Figure 3 to the *in-situ* measurements, as shown in the right hand panel of Figure 3, we can determine the time history of the cusp density profile and thus determine whether the injection is steady-state or impulsive. In this case, the echo time delay shows a peak virtual range of 1.2 RE) at about 45 kHz, consistent with a shallow density gradient "shelf" at that frequency, and a shallow area from 50–90 kHz, consistent with a steep density gradient. This sweep was taken at around 0611, May 11, 2000. Comparing the estimated density profile with the *in-situ* measurements on the right shows a good agreement with the density profile observed an hour later. Thus, at least in this case, the injection mechanism is quasi-steady. However, from sweep to sweep the sounding traces show considerable variability, so that the injection mechanism is clearly not time-independent.

The cusp density profile obtained from Figure 3 can be used to determine the means of particle injection. The white line in the spectrogram represents a broad cusp density profile, which is consistent with a diffusive entry. The merging cusp entry predicts a cusp density profile that is very steep on the equatorward side and broad on the poleward side. The spectrogram on the right side of Figure 3 (see also Figure 1) shows in fact a steep equatorward gradient (at about 0730) and a broad profile on the poleward side (from 0630–0720). Thus, these profiles are consistent with entry from magnetic merging.

WHISTLER MODE ECHOES

When the RPI transmitted frequency falls below the local electron cyclotron frequency, the transmitted wave can propagate as a whistler mode wave. When IMAGE is well within the plasmasphere, whistler mode echoes are received, allowing determination of low-altitude electron density structures. Figure 4 shows whistler mode returns (falling trace from 10–40 kHz), and a plasmapause echo trace from 80–200 kHz.

CONCLUSIONS

The RPI provides a wealth of information about the electron density structures and boundary locations of many features in the Earth's magnetosphere (see Green *et al.*, 2000). Initial RPI sounding observations demonstrate that even during relatively intense natural emissions, such as solar type III radio bursts, echoes can be observed from the plasmasphere at distances of 3 RE or greater from the target. These are the first radio soundings at such large radial distances within the magnetosphere.

The RPI also operates in a passive mode in order to receive natural magnetospheric emissions. Because RPI uses the longest dipole antennas ever flown, and has ultra low noise radio receivers, as well as it is located on an electro-magnetically clean spacecraft, RPI is providing some of the most unique natural emission measurements ever made within the magnetosphere. The passive operations help to eliminate possible confusion about the reception of echoes from active RPI transmissions, and place the sounder echo measurements into a familiar context.

These types of observations provide very precise measurements of the plasma characteristics within the Earth's magnetosphere and should have a dramatic effect on improving our density models under a variety of magnetospheric conditions.

Acknowledgements. The work at University of Massachusetts Lowell and Rice University was supported by NASA under subcontracts to Southwest Research Institute and at Raytheon ITSS under NASA contract NASW–97002.

REFERENCES

[1] The IMAGE Mission / Ed. J. L. Burch.–Reprinted from Space Sci. Rev.–2000.–**91**.–No. 1–2.

[2] *Green J. L., Benson R. F., Fung S. F., et al.* Radio Plasma Imager simulations and measurements // Space Sci. Rev. special issue on the IMAGE mission.–2000.–**91**.–P. 361–389.

[3] *Oya H., Morioka A., Kobayashi K. , et al.* Plasma wave observation and sounder experiments (PWS) using the Akebono (EXOS-D) satellite – Instrumentation and initial results // J. Geomagn. Geolelectr.–1990.–**42**.–P. 411–442.

[4] *Reinisch B. W.* Modern Ionosondes // Modern Ionospheric Science / Eds. H. Kohl, R. Rüster, and K. Schlegel.–European Geophys. Soc., 37191 Katlenburg-Lindau, Germany, 1996.–P. 440–458.

[5] *Reinisch B. W., Sales G. S., Haines D. M., et al.* Radio wave active Doppler imaging of space plasma structures: angle-of-arrival, wave polarization, and Faraday rotation measurements with RPI // Radio Sci.–1999, Nov.–Dec.–**34**.–P. 1513–1524.

[6] *Reinisch B. W., Haines D. M., Bibl K., et al.* The Radio Plasma Imager investigation on the IMAGE spacecraft // Space Sci. Rev. special issue on the IMAGE mission.–2000a.–**91**.–P. 319–359.

[7] *Reinisch B. W., Huang X., Haines D. M., et al.* First Results from the Radio Plasma // Geophys. Res. Letts.–2000b.–submitted.

EXPLORATION OF THE SOLAR SYSTEM WITH THE TWO-CHANNEL FOCAL REDUCER AT THE 2m-RCC TELESCOPE OF PIK TERSKOL OBSERVATORY

K. Jockers[1], **T. Credner**[1], **T. Bonev**[2], **N. Kiselev**[3], **P. Korsun**[4], **I. Kulyk**[4], **V. Rosenbush**[4], **A. Andrienko**[5], **N. Karpov**[5], **A. Sergeev**[5], **and V. Tarady**[5]

[1] *Max-Planck-Institut für Aeronomie*
D-37191 Katlenburg-Lindau, Germany
e-mail: jockers@linmpi.mpg.de

[2] *Institute of Astronomy of Bulgarian Academy of Sciences*
Tsarigradsko Chausée 72, 1784 Sofia, Bulgaria

[3] *Astronomical Observatory of Kharkiv National University*
Sumskaya St., 61022 Kharkiv, Ukraine

[4] *Main Astronomical Observatory, NAS of Ukraine*
27 Akademika Zabolotnoho St., 03680 Kyiv, Ukraine

[5] *International Center for Astronomical and Medico-Ecological Research*
27 Akademika Zabolotnoho St., 03680 Kyiv, Ukraine

In 1996 the Two-Channel Focal Reducer of the Max-Planck-Institute for Aeronomy has been brought to Pik Terskol Observatory for use at the 2m-Zeiss-RCC telescope. We describe the instrument and its possibilities. Up to now it has been used for the following solar system projects: astrometry and photometry of the inner satellites of Jupiter, imaging the Io torus with a tunable Fabry-Perot interferometer, photometry and polarimetry of asteroids, imaging photometry and polarimetry of cometary dust and imaging photometry of ions and neutral molecules in comets. These projects are briefly described.

INTRODUCTION

Telescopic studies of solar system objects, in particular of comets, are difficult to schedule at modern astronomical observatories, because the appearance of such objects frequently is not known sufficiently long in advance to provide sufficient time for a regular proposal of observing time. A contract between the Max-Planck-Institute for Aeronomy (MPAe) and the International Center for Astronomical and Medico-Ecological Research (Center AMER), valid until the end of 2002, allows the MPAe, if needed, access to the 2m-Zeiss-RCC-Telescope at Pik Terskol Observatory on short notice. The MPAe has brought its Two-Channel Focal Reducer to Pik Terskol Observatory. This equipment can be made available also to other interested parties. Therefore it seems useful to describe this instrument in some detail and to give an account of the investigations performed up to now under the initiative of the MPAe.

THE TWO-CHANNEL FOCAL REDUCER

The focal reducer principle has first been described by Courtès [4], who also coined the name "réducteur focal". A focal reducer adapts the imaging elements of the detector to the characteristic size of the object or of the seeing disk. The Two-Channel Focal Reducer of the MPAe was built mainly for observations of cometary plasma but has proven useful for many other tasks [7]. Fig. 1 shows the optical arrangement. Behind the RC (Cassegrain) focus the telescope beam is recollimated by a lens collimator. A color dividing (dichroic) mirror reflects the blue part of the spectrum and transmits the red part. In each "channel" camera lenses form reduced images of the Cassegrain focal plane, which are recorded by two CCD systems. Table 1 provides the main parameters of the optical system. Dispersive or polarizing optical elements can be put in the parallel beam either before or after the color divider. Optical elements to be placed in front of the color divider are two tunable and one fixed gap Fabry-Perot etalons and a polarizing beamsplitter. They affect both channels of the instrument. Optical elements put into the parallel beam after color separation are filters, grating prisms, and solid fused silica etalons. A list of available filters is provided in Table 2. In order to obtain an unvignetted image on the detector it is necessary that the entrance pupil of the camera lens coincides with the exit pupil

Invited paper.

of the collimating system. This condition is difficult to satisfy as the dispersive elements and the color divider need some space. In order to reduce vignetting to a minimum, if no optical elements are on the telescope side of the color divider, the lower part of the instrument can be moved toward the Cassegrain focal plane in order to minimize the distance between exit pupil of collimator and entrance pupil of the camera lenses at least in this case. An automatized offset guider is available, which can follow moving objects like comets [12].

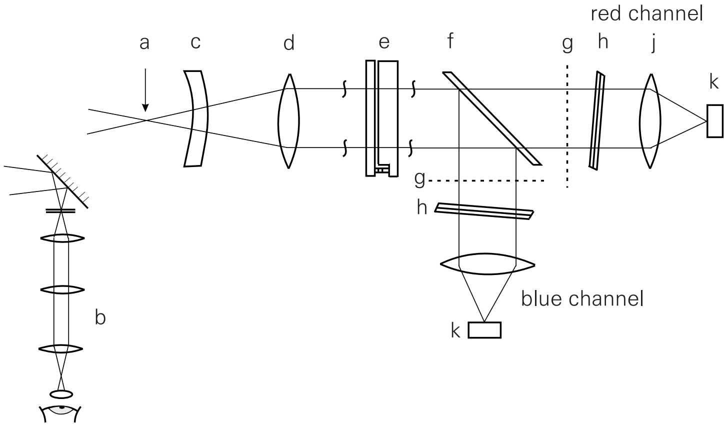

Figure 1: Optical scheme of the Two-Channel Focal Reducer. (a) Cassegrain focal plane, (b) offset guider, (c) field lens, (d) collimator, (e) Fabry-Perot etalon or four-beam Wollaston prism, (f) color divider, (g) Lyot stop (not always present), (h) filter, (j) camera lens, (k) CCD detector. If position (e) is empty, the right part of the instrument can be moved to the left toward the Cassegrain focal plane in order to reduce vignetting

Table 1: Main parameters of the optical system

Collimator	f = 400 mm, exit pupil diameter 50 mm.			
	reflecting	transmitting	reflecting	transmitting
Color dividers	λ <390 nm	425 nm< λ	λ <445 nm	490 nm< λ
(two dividers per row are listed)	λ <500 nm	570 nm < λ	λ <520 nm	580 nm< λ
	500 nm< λ <670 nm	800 nm< λ	all λ (mirror)	
	blue arm		red arm	
Camera lenses (f=140mm)	355 nm< λ <510 nm		420 nm< λ <700 nm	
	420 nm< λ <700 nm		590 nm< λ <1000 nm	
CCDs:	blue sensitive 512 × 512 pixel		blue sensitive 576 × 385 pixel	
Pixel size (sky projection)	0.027 mm (1.00 arcsec)		0.022 mm (0.81 arcsec)	
Sky field	7.8 × 7.8 arcmin		7.8 × 5.2 arcmin	
Polarimetry field	1.3 × 1.3 arcmin		1.3 × 1.3 arcmin	

The instrument has several observing modes. The simplest mode is the mode of *filter imaging*, where broad-band or interference filters are placed into each arm of the focal reducer and the appropriate color divider (see Table 1) is selected. Note that it is not possible to use adjacent UBVRI filters at the same time, one can either use U and V or B and R simultaneously. Presently there is no color divider available which allows simultaneous imaging in V and I, only B and I can be imaged at the same time.

The device allows *long slit spectrography* with a grating prism (transmission grating cemented on a prism). In this mode a slit is placed at the Cassegrain focal plane. The available grating prism (600 lines/mm) works in the blue arm only. It has a straight-through (center) wavelength of 392 nm and provides a resolution of 0.64 nm in the range 355–460 nm. Often such a setup is called faint object spectrograph as it is possible to take an image of the field, identify a faint object, put it on the slit with a telescope offset, insert the slit and take a spectrum. This mode has been used only rarely with the Two-Channel Focal Reducer.

More experience exists with *interferometry using Fabry-Perot interferometers (FPIs)* [6]. Table 3 presents the characteristics of the etalons. The two tunable FPIs provide a single broad fringe covering a large part of the CCD frame and can be looked upon as tunable narrow-band filters with about 3-4 Å FWHM (full width at half maximum). By proper selection of the interference order one can select wavelength pairs for simultaneous

Table 2: Filters

Filter name	λ_0^a [nm]	τ_{max}^b	FWHM[c] [nm]	FWTM[d] [nm]	λ_{leak}^e ($\tau > 0.001$) [nm]	τ_{max}^f (leak)	D[g] [mm]	+ additional blocking filter
Wide band filters								
DUG11	338	0.832	75	93			60	
DUG12	338	0.828	75	92			80	
BG24/10	(< 350) - 449	0.936			655 - (> 900)	0.68	80	+ BG39/2
BG24/39	(< 350) - 458	0.753					80	
BG39/2	472	0.928	235				80	
BG39/2	472	0.928	235				60	
B	431	0.946	95	128	636 - 660	0.002	80	+ BG39/2
					754 - (> 900)	0.79		
Gunn G	519	0.818	65	106			80	
V	531	0.920	102	270			80	
R	680	0.948	111	175			80	
I	797	0.964	153	180			80	
Gunn Z	821 - (> 900)	0.969					80	
HalleUV	390	0.783	103	146			80	
LC660	(< 350) - 665	0.949			774 - (> 900)	0.89	80	
LC661	(< 350) - 669	0.950			775 - (> 900)	0.80	80	
RG66	595 - (> 900)	0.759			(< 350) - 516	0.018	80	
RX	694	0.950	79	101			80	
UG11/4	324	0.824	91	116	691 - 737	0.007	80	
Narrow band filters								
IF358	358.1	0.751	11.4	16.1	673 - (> 900)	0.32	80	+ DUG
IF369	369.3	0.586	9.8	14.0	673 - (> 900)	0.28	80	+ HalleUV
IF390	389.4	0.672	10.5	15.3	655 - (> 900)	0.56	80	+ BG39/2
IF404	403.5	0.678	9.8	13.9	696 - (> 900)	0.017	80	+ BG39/2
IF425	424.2	0.593	6.4	8.9	695 - (> 900)	0.017	80	+ BG39/2
IF426	425.9	0.740	3.7	6.4	521 - 681	0.075	80	+ BB
IF444	443.5	0.808	4.2	6.0	361 - 371	0.003	80	+ BB
					555 - 688	0.54		
IF501	500.2	0.701	4.1	9.2			80	
IF510	509.4	0.734	4.4	6.4			80	
IF590	589.4	0.591	2.5	3.5			80	
IF614	614.9	0.797	3.2	5.7	734 - 766	0.029	80	+ LC660
IF620	619.5	0.678	3.7	5.9	799 - 801	0.002	80	
IF629	629.1	0.902	2.9	5.2	779 - 787	0.003	80	
IF631	630.8	0.796	3.1	4.4			80	
IF642	641.6	0.580	2.6	3.8			80	
IF658	657.2	0.867	3.2	6.0			80	
IF660	658.5	0.805	28.8	35.4			80	
IF662	662.1	0.881	5.9	8.9			80	
IF667	666.2	0.910	5.5	8.2			80	
IF672	671.9	0.833	3.3	6.1			80	
IF890	888.5	0.988	29.0				80	
IF953	953.7	0.65	1.0		832 - 834	0.004	60[h]	
IF360	359.7	0.750	3.0	4.1	420 - (> 900)	0.92	60	+ DUG
IF368	367.3	0.773	2.5	3.4	430 - (> 900)	0.92	60	+ DUG
					510 - 521	0.004		
					582 - (> 900)	0.86		
IF373	373.1	0.395	3.2	6.3	429 - 432	0.001	60	+ HalleUV
					672 - (> 900)	0.42		
IF407	406.8	0.498	2.3	6.2	690 - (> 900)	0.85	60	+ BG39/2
IF426	425.3	0.683	3.2	5.9	695 - (> 900)	0.82	60	+ BG39/2
IF443	443.2	0.797	4.4	7.9	726 - (> 900)	0.81	60	+ BG39/2

[a] center wavelength
[b] maximum transmission
[c] full width at half of maximum transmission
[d] full width at one thousandth of maximum transmission
[e] range of undesirable transmission ("leak")
[f] maximum of undesirable transmission
[g] filter diameter
[h] filter fits only into red arm

Table 3: Fabry-Perot-interferometers

Name	kind	useful λ range	reference λ [nm]	free spectral range [nm]	mounted
Queensgate visual	tunable	410-700	627	5.8	before beamsplitter
Queensgate blue	tunable	355-510	374.7	4.3	before beamsplitter
CSIRO visual	fixed airgap	410-700	620	0.21	before beamsplitter
CSIRO red	fused silica	450-700	615	0.26	red arm filter slide
CSIRO blue	fused silica	350-530	400	0.17	blue arm filter slide

imaging in both arms [7]. The data reduction has been described in [1] and [19]. The fixed-gap FPIs provide fringe systems and can be used for radial velocity measurements. The fused silica ones are tilted with respect to the telescope beam by 4°, in order to avoid internal reflections and to adapt the finesse of the etalons to the spatial resolution of the CCD matrix. The tunable and the fused silica FPIs can be used in tandem.

Of particular interest is the *imaging polarimetry* mode. It is shown in Fig. 2 and has been described in [5]. An assembly of four Wollaston prisms, aligned parallel to each other with an accuracy $< \lambda/4$ is brought in the parallel beam on the telescope side of the color divider in order to let it affect both channels. Two of the four Wollaston prisms are identical pairs, *i.e.*, optically there are only two different Wollaston prisms, one that splits the beam into polarization directions 0° and 90°, and the other into polarization directions ±45°. In this way the exit pupil of the telescope is split in two halves and four small images with polarization directions 0°, 90°, +45°, and −45° are produced on the CCD matrix simultaneously in a single exposure. In rapidly changing objects like comets this simultaneity is advantageous but there are disadvantages: The point spread function of the pair 0° and 90° differs from the pair +45° and −45°. This creates problems if the telescope is not perfectly in focus. The basic limitation, however, comes from the inaccuracy introduced by the flat-fielding process and, ultimately, from the high count rate necessary for imaging polarimetry. Because of the Poisson statistics inherent in the count rate of a CCD, if we want an accuracy of 0.1% we need 10^6 counts per pixel, which is very hard to achieve on an astronomical object. A similar accuracy is necessary in the flat fields. Experiments show that an accuracy of the degree of polarization significantly better than 1% is very hard to achieve.

In Fig. 1 we mention the Lyot stops, which allow to use the instrument in *coronagraph mode*. A bright object in the field can be put behind a dark mask or (better) absorbing neutral density glass, located at the Cassegrain focal plane. The Lyot stop is positioned at the location of the exit pupil (image of primary mirror) formed by field lens (c) in Fig. 1 (actually, in our instrument we have two Lyot stops, one in each arm). The Lyot stop covers the rims of both, secondary and primary mirror and the spider holding the secondary mirror. In this way the diffraction spikes of the bright object behind the mask are significantly reduced. Faint detail close to the bright object may become observable. Presently the coronagraph mode is possible in combination with all other observing modes except of polarization. The Wollaston prism assembly produces 4 different images of the telescope mirror. To cover them all would introduce somewhat larger light losses.

PROJECTS CONDUCTED AT PIK TERSKOL SINCE 1996

Astrometry and photometry of the inner satellites of Jupiter and the Saturnian satellite Phoebe

The coronal skies at Pik Terskol Observatory combined with low atmospheric turbulence provide good conditions for the investigation of faint objects close to bright ones. The observations are conducted with the focal reducer in coronagraph mode. We have been able to observe the inner moons of Jupiter Methis, Amalthea and Thebe and obtained their astrometric positions and brightness as a function of phase angle ([18], [20]). Such observations are most promising in case of Methis, which so far has not been observed at small phase angles.

Io torus

The Io torus is a plasma ring consisting almost exclusively of oxygen and sulphur ions encircling Jupiter at about the distance of the satellite Io. It is created mostly by SO_2 molecules from Io, which are dissociated and ionized by electrons in the Jovian magnetosphere. They radiate in much the same way as in gaseous nebulae. The work conducted at Pik Terskol is an extension of [19]. One of the aims is to support measurements of the space probes Galileo and (in 2000) Cassini. Using the coronagraph setup and the visual tunable Fabry-Perot interferometer we observe the red [SII] doublet at 6716.4 and 6730.9 Å and the lines of [SIII] at 9530.9 and 6312.1 Å. The lines of [SIII] show the hotter material and the line ratio allows to derive the electron temperature

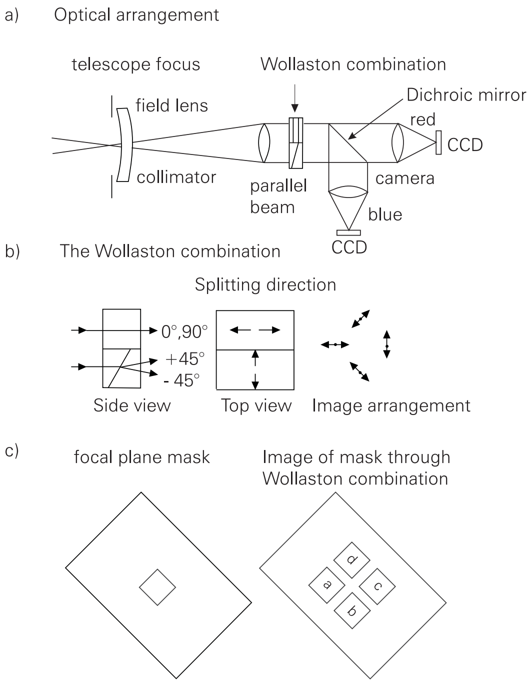

Figure 2: Optical scheme of the Two-Channel Focal Reducer in polarimetric mode

while the [SII] lines show the cooler material and the line ratio provides electron density. Morphological details observed under excellent seeing conditions indicate a warping of the torus.

Asteroid polarimetry and photometry

Asteroid regolith has optical properties surprisingly similar to cometary dust. Since 1996 two programs concerning asteroids have been conducted, polarimetric observations of asteroid 2100 Ra-Shalom at large phase angle ([13], [14]), and photometric and polarimetric observations of asteroid 64 Angelina near opposition [23].

Cometary dust

Since 1996 we have observed comets C/1995 O1 (Hale-Bopp), C/1996 Q1 (Tabur), 46P/Wirtanen, 21P/Giacobini-Zinner, C/1998 U5 (Linear), C/1999 H1 (Lee), C/1999 J3 (Linear), and C/1999 S4 (Linear). Most of these comets were observed through the blue and red continuum filters at 443 nm and 642 nm. The passbands of these filters are considered free from emissions of cometary molecules or ions and show only the solar light, scattered by the cometary dust particles. If possible, also imaging polarimetry has been done in these passbands. Some comets, in particular the larger ones like Comet Hale-Bopp, show a structured dust coma with “jets” and “shells”, which are visible in the polarization and color images as well. In [10] it is concluded that the jet particles have optical properties like submicron grains but experience solar radiation pressure similar to larger grains. This points to the aggregate nature of the jet particles (see also [21], [22]). Another important result is the negative wavelength gradient of polarization found in Comet 21P/Giacobini-Zinner, which distinguishes this comet from almost all other comets ([15], [16]).

Cometary gas and plasma

We have observed cometary gas and plasma in all comets mentioned in the previous paragraph, except C/1999 H1 (Lee). The work includes derivation of the water production rate from observations of the [OI] 6300 Å line with Fabry-Perot etalon CSIRO red (Table 3), using the radial velocity of the comet to separate the cometary emission from terrestrial airglow [11]. The water production rate was also derived from observations of H_2O^+ ([24], [8], [11]). Comet 46P/Wirtanen, the target of the ESA Rosetta mission, was observed as well and a water production rate has been determined ([9], [24]). The cosmochemically important ratio of H_2O^+/CO^+ has been derived in [3] and [8] for several comets. Plasma velocities have been published in [2] and [3]. CN and NH_2 maps of Comet C/1999 J3 (Linear) have been analyzed in [17]. For more details we refer the reader to two other contributions to this conference, [11] and [17].

REFERENCES

[1] *Bonev T., Jockers K.* H_2O^+ ions in the inner plasma tail of comet Austin-1990-V // Icarus.–1994.–**107**.–P. 335–357.

[2] *Bonev T., Jockers K., Credner T.* Comet Hale-Bopp: velocity field of ions from Fabry-Perot imaging // Earth, Moon and Planets.–1997.–**77**.–P. 245–252.

[3] *Bonev T., Jockers K., Korsun P., et al.* H_2O^+ and CO^+ in comet C/1999 J3 (Linear) // Bulgarian Journal of Physics.–2000.–submitted.

[4] *Courtès G.* Méthodes d'observation et étude de l'hydrogène interstellaire en émission // Ann. d'Astrophys.–1960.–**23**, N 2.–P. 115–217.

[5] *Geyer E. H., Jockers K., Kiselev N. N., Chernova G. P.* A novel quadruple beam imaging polarimeter and its application to Comet Tanaka-Machholz 1992 X // Astrophys. and Space Sci.–1996.–**239**.–P. 259–274.

[6] *Jockers K.* Astronomical observations of comets and the Io torus using Fabry-Perot-Interferometry // Tridimensional Optical Spectroscopic Methods in Astrophysics: IAU Coll. 149 / Eds G. Comte and M. Marcelin.–San Francisco: ASP Conf. Ser., 1995.–**71**.–P. 182–187.

[7] *Jockers K.* A two-channel focal reducer for small (diameter $\geq$ 1 m) telescopes // Exper. Astron.–1997.–**7**.–P. 305–318.

[8] *Jockers K., Bonev T., Credner T.* Observations of ions in comets: A contribution towards understanding the comet-solar wind interaction // Astrophys. and Space Sci.–1999.–**264**.–P. 227–234.

[9] *Jockers K., Credner T., Bonev T.* Water ions, dust and CN in comet 46P/Wirtanen // Astron. and Astrophys.–1998.–**335**.–P. L56–L59.

[10] *Jockers K., Rosenbush V. K., Bonev T., Credner T.* Images of polarization and colour in the inner coma of comet Hale-Bopp // Earth, Moon and Planets.–1997.–**78**.–P. 373–379.

[11] *Jockers K., Bonev T., Korsun P., et al.* Water production of comets derived from observations of [OI] (6300 Å) and H_2O^+ (6150 Å): Comets C/1998 U5 (Linear) and C/1999 J3 (Linear) // this issue.–P. 262–265.

[12] *Karpov N. V., Jockers K.* Information support of observations at the 2-m telescope of Pik Terskol Observatory // Kinematics and Physics of Celestial Bodies.–2000.–**16/4**.–in print.

[13] *Kiselev N. N., Rosenbush V. K., Jockers K.* Polarimetry of asteroid 2100 Ra-Shalom. A comparison of polarization-phase dependences for C- and S-type asteroids and comets // Astron. Vestnik.–1999.–**33**.-P. 222–230. (in Russian).

[14] *Kiselev N. N., Rosenbush V. K., Jockers K.* Polarimetry of asteroid 2100 Ra-Shalom at large phase angle // Icarus.–1999.–**140**.–P. 464–466.

[15] *Kiselev N. N., Jockers K., Rosenbush V. K., et al.* Anomalous wavelength dependence of polarization of comet 21P/Giacobini-Zinner // Planet. and Space Sci.–2000.–**48**.–P. 1005–1009.

[16] *Kiselev N., Jockers K., Rosenbush V. K.* Negative wavelength gradient of polarization of Comet 21P/Giacobini-Zinner as an indicator of organic matter in its dust particles // this issue.–P. 266.

[17] *Korsun P. P., Jockers K.* CN and NH_2 atmospheres of Comet/1999 J3 (Linear) // this issue.–P. 267–268.

[18] *Kulyk I., Jockers K., Karpov N., Sergeev A.* Near-infrared photometric observations of the inner Jovian satellites // this issue.–P. 231–233.

[19] *Küppers M., Jockers K.* A multi-emission study of the Io plasma torus // Icarus.–1997.–**129**.–P. 48–71.

[20] *Ledovskaya I., Jockers K., Karpov N., Sergeev A.* Astrometric CCD observations of Jovian inner satellites Thebe, Amalthea, and Saturnian satellite Phoebe in the 1998 opposition // Kinematics and Physics of Celestial Bodies.–1999.–**15/6**.–P. 483–485.

[21] *Petrova E. V., Jockers K., Kiselev N. N.* Light scattering by aggregates with sizes comparable to the wavelength: an application to cometary dust // Astron. Vestnik.–2000.–in press. (in Russian).

[22] *Petrova E. V., Jockers K., Kiselev N. N.* Light scattering by aggregates with sizes comparable to the wavelength: an application to cometary dust // Icarus.–2000.–in press.

[23] *Rosenbush V. K., Kiselev N. N., Jockers K., et al.* Optical polarimetry of the Galilean satellites, Iapetus, and 64 Angelina near opposition // this issue.–P. 227–230.

[24] *Wegmann R., Jockers K., Bonev T.* H_2O^+ ions in comets: models and observations // Planet. and Space Sci.–1999.–**47**.–P. 745–763.